Robotic *Elytra:* Insect-Inspired Protective Wings for Resilient and Multi-Modal Drones

Charalampos Vourtsis, *Student Member, IEEE*, William Stewart, *Member, IEEE*, and Dario Floreano, *Senior Member, IEEE*

***Abstract*—Winged drones that fly in close proximity to obstacles or that are capable of aerial and terrestrial locomotion can benefit from protective systems that prevent damage to delicate aerial structures. Existing protective solutions focus on multi-copter drones and consist of adding structures, such as cages, mechanisms and instruments that add weight and drag. Here we describe a protective strategy for winged drones that mitigates the added weight and drag by means of increased lift generation and stall delay at high angles of attack. The proposed structure is inspired by the wing system found in beetles and consists of adding an additional set of retractable wings, named *elytra*, which can rapidly encapsulate the main folding wings when protection is needed.**

***Index Terms*—Biologically-inspired robots, mechanism design.**

I. Introduction

PROTECTION from collisions has been extensively studied for multi-rotor drones and terrestrial robots. Among the most common protective strategies is to completely enclose the vehicle in a cage [1]–[5], or partially surround it in protective bumper structures [6], [7]. However, these solutions are not practical for fixed-wing drones as the enclosing structure would interfere with the lift generating capabilities of the wings. As a result, alternative strategies are required for winged drones. The most common strategy consists of fabricating the robot out of impact-resilient foam materials (such as Expanded Polypropylene-EPP, e.g.). These foams can sustain high impact loads, but remain susceptible to puncture. Simply using impact resilient materials in this manner also leaves the extended wing structure exposed to damage from contact with the environment [8]. Passively folding wings can be retracted to avoid collisions, but in the event of a collision with sharp surfaces they are still vulnerable to being torn [9]. State of the art, sub-gram micro-aerial robots display collision resilience properties although their constantly exposed wings and fuselage allow for continuous structural degradation with each collision [10]. Multi-modal locomotion drones such as DALER [11] can even use their shape-shifting mechanisms to absorb impact energy at contact, but they too remain vulnerable to damage from penetration by spicular surfaces. Despite increased resilience, folding wing solutions remain vulnerable to damage because even when folded, their wings are exposed to contact.

Inspired by the protective structure of beetles, here we describe a novel protective mechanism for winged drones that protects folded wings from puncture by enclosing them in a protective shell, which also generates lift during flight to offset its added weight. *Coleoptera* (beetles) are insects that have exhibited resilience for more than 60 million years to the point that today they represent approximately 40% of all living insects [12] (Fig. 1 (A)). Anatomically, flying beetles are characterized by a protective exoskeleton and a dual-wing system; hind-wings and the *elytra* (Fig. 1(B)). The hind-wings are the primary source of lift generation and are soft, foldable, membrane structures. The *elytra* are multi-functional hardened shells that can fully encapsulate the folding wings when not in flight and provide collision and penetration resilience [13]. When in flight, the *elytra* work in synergy with the hind-wings to generate additional lift to support their weight [14] and delay stall [15].

In this letter, we show that a dual-wing system, (hind-wings and *elytra*), can be used for small winged drones to provide protection from puncture while mitigating the added drag and weight costs that other protective solutions, such as cages, suffer from. In our solution, the *elytra* completely encompass the folded hind-wings, protecting them from spicular surfaces or obstacles in the vicinity of the aircraft. Specifically, our approach (i) generates additional lift to partially offset the *elytra* weight in cruise flight (ii) improves the lift to drag ratio at high angles of attack compared to single wing configurations and (iii) delays stall. To investigate these benefits, we performed aerodynamic experiments on a simplified test article composed of a fixed wing and *elytra* that could change their dihedral and angle of incidence. As beetles are of small size and weight (NAV scale shown in Fig. 2) compared with most commercial UAVs (MAV scale in Fig. 2), we scaled up the geometric parameters of the insect to fit the size of a common MAV (Fig. 2) [12]. This scale of vehicle is useful for roboticists as it is small enough to be cheap and easy to manufacture robots, while large enough for

Manuscript received June 24, 2021; accepted October 21, 2021. Date of publication October 27, 2021; date of current version November 10, 2021. This letter was recommended for publication by Associate Editor B. Mazzolai and Editor X. Liu upon evaluation of the reviewers' comments. This work was supported in part by the European Union's Horizon 2020 Research and Innovation Programme under Marie Skłodowska-Curie Grant Agreement 754354, in part by Swiss National Science Foundation through the National Centre of Competence in Research (NCCR), and in part by European Union's Horizon 2020 Research and Innovation Programme under Grant Agreement ID: 871479 AERIAL-CORE. *(Corresponding author: Charalampos Vourtsis.)*

The authors are with the Laboratory of Intelligent Systems, Ecole Polytechnique Federale de Lausanne, CH1015 Lausanne, Switzerland (e-mail: harry.vourtsis@epfl.ch; william.stewart@epfl.ch; dario.floreano@epfl.ch).

This letter has supplementary downloadable material available at https://doi.org/10.1109/LRA.2021.3123378, provided by the authors.

Digital Object Identifier 10.1109/LRA.2021.3123378

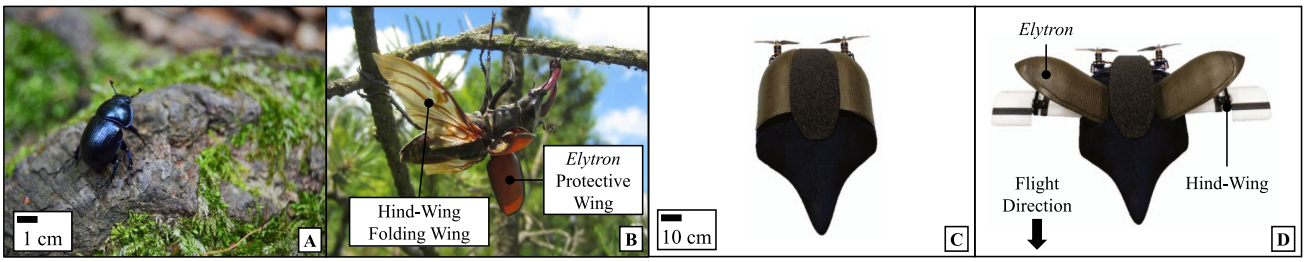

Fig. 1. (A) A *Scarabaeidae* beetle in its natural habitat, perching on a branch, in protective configuration with the hind-wings folded under the protective *elytra* [16]. (B) Wing anatomy of a *Scarabaeidae* beetle. The figure displays the system of the hind-wings and the *elytra* in a *Scarabaeidae* beetle [17], [18]. (C) HercuLIS, the drone described in this article, with retracted wings. Hybrid carbon-Kevlar *elytra* encapsulate the fragile folding wings. (D) HercuLIS with deployed wings for horizontal flight.

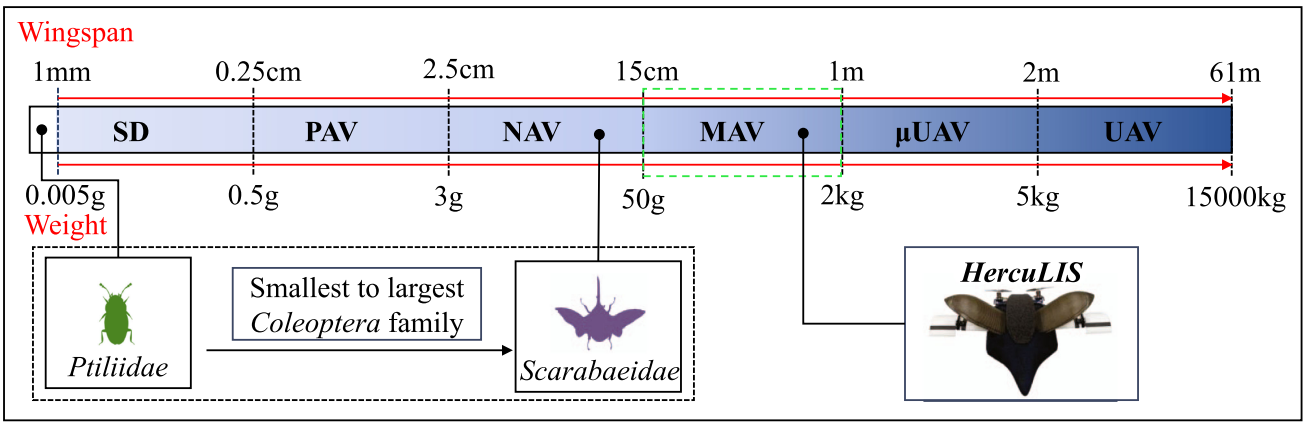

Fig. 2. The morphology and size of *Coleoptera*. Wingspan and weight comparison of existing drone sizes (SD Smart-Dust, PAV-Pico Aerial Vehicle, NAV-Nano Aerial Vehicle, MAV-Micro Aerial Vehicle, UAV-Micro Unmanned Aerial Vehicle, UAV-Unmanned Aerial Vehicle) with the smallest and the largest size of *Coleoptera* families. The drone scale was adapted from [19]. The green box indicates the weight and size category (MAV) that HercuLIS belongs to.

the robots to be capable of carrying payloads. The proposed hind-wings and *elytra* system resemble a biplane configuration, so we also examined how well the existing biplane model can describe the lift and drag generation of our dual-wing system. Finally, we validated the proposed design with a free-flying, multi-modal, winged drone code named HercuLIS that can fly and locomote on the ground using wheels. On the ground, the *elytra* cover the folded wings and electronics to protect them. During flight, the *elytra* and the hind-wings unfold to produce lift.

The rest of the letter is organised as follows. In the second section, we explain the rationale behind the geometric design of the hind-wings and the *elytra* while we discuss the aerodynamic modeling and the aerodynamic experiments in the wind tunnel. Then in the third section, we describe the integration of the hind-wings and *elytra* system into HercuLIS, and outdoor experiments. Finally, in the fourth and final section, we discuss possible applications and extensions of the proposed system.

II. Aerodynamic Characterization

To investigate whether the aerodynamic advantages of the beetle hind-wing and *elytra* system can be translated to a drone, we performed experiments in an open wind tunnel using a simplified test article. As the insect flies, it varies its *elytra* dihedral and *elytra* angle of incidence, thus, we examined how these angles could affect lift and drag forces for a given wing configuration. The test article consists of a dual-wing system that captures the relevant geometric parameters of the beetle. We scaled the beetle wing geometric ratios (length and chord) such that they fit the dimensions of a standard MAV platform (Fig. 2), [12]. These scaled parameters were used for the chord and wing length of the *elytra* and the hind-wings. The relative distances between the hind-wings and the *elytra* (parameters x,z in Table I and Fig. 3) were designed in CAD for achieving the different configurations of *elytra* angle of incidence and dihedral angle that we chose to investigate while reducing structural weight (Fig. 3(B, C)). For clarity, the angle of incidence refers to the angle between the hind-wing and *elytra* (α_e in Fig. 3), while the angle of attack refers to the angle between the hind-wing and the incident airflow (α in Fig. 3).

The main wings of the test article consisted of hot-wire cut polystyrene foam reinforced with a rectangular carbon fiber beam. The main wings had a total span of 1 m and chord of 15 cm. The *elytra*, as well as the interface between the test article and the load sensor were fabricated from polyamide (PA) and acrylonitrile butadiene styrene (ABS) respectively. The *elytra* were 3D printed by a EOSINT P-395 printer (ABS) and the interface between the test article and the load sensor by a Stratasys Dimension Elite printer (PA). The *elytra* were mounted to two

TABLE I
EXPERIMENTAL CONSTANTS AND VARIABLES ADJUSTED FROM BEETLES TO ROBOTS

Environment Constants and Variables	**Symbol**	**Range / Value**
Angle of Attack	a	$-4^\circ \leq a \leq 20^\circ$
Wind-Speed	v_{inf}	8 m/s
Hind-Wings Constants and Variables	**Symbol**	**Range / Value**
Hind-Wing Length	w_m	0.5 m
Hind-Wing Chord	c_m	0.17 m
Hind-Wing Airfoil	af_h	E63
***Elytra* Constants and Variables**	**Symbol**	**Range / Value**
Elytron Wing Length	w_e	0.28 m
Elytron Chord	c_e	0.15 m
Elytron Airfoil	af_e	Cambered Plate
Elytra Hind-Wings Vertical Distance	z	0.05 m
Elytra Hind-Wings Horizontal Distance	x	0.04 m
Elytron Angle of Incidence	a_e	$-20^\circ \leq a \leq 20^\circ$
Elytron Dihedral Angle	d	$12^\circ \leq a \leq 27^\circ$

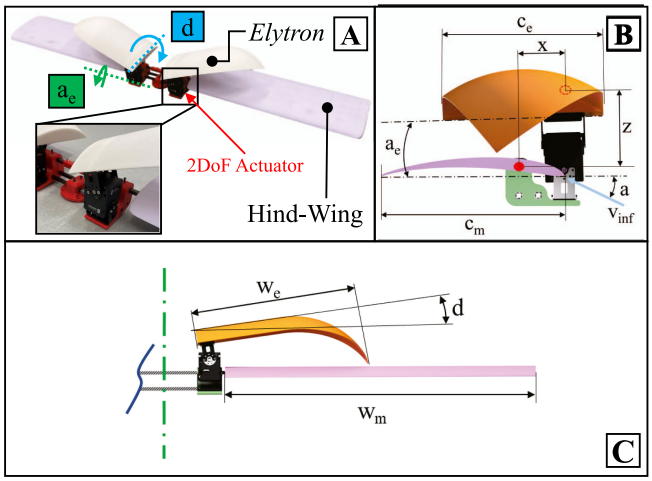

Fig. 3. The aerodynamic test article. (A) A simplification of the hind-wings, *elytra* wing system to investigate the aerodynamic performance at different angle configurations. The test article is composed of a fixed-wing and *elytra* that are mounted on 2 DoF (Degrees of Freedom) actuators. (B - C) The relative positioning of the *elytra* and the hind-wings in the x and z axis was dictated by the insect geometry and physical geometric limitations e.g. actuator size.

2-axis servo actuators (Robotis Dynamixel 2XL430-W250-T). The servo motors were communicated with through serial (TTL) protocol and controlled by a laptop using custom python scripts.

We performed wind tunnel experiments in an open-jet wind tunnel (WindShape [20], [21]). The flow speed was measured with a one dimension (1D) flow meter which was used to tune the wind tunnel to mean airspeed of 8 m/s. Turbulence was measured to be less than 2%. The wind tunnel testing cross-section was 1.7 m wide 1.5 m tall for a total test section area of 2.55 m^2. The angle of attack was measured by the robotic arm, while the angle of incidence and the dihedral angle were measured by the position feedback of the servo motors. The uncertainty in angle of attack was estimated to be $< 0.2^\circ$ while in the servo motor angles $< 0.5^\circ$. The indicated airspeed corresponds to Reynolds numbers (Re) of 95,727 for the hind-wings and 84,465 for the *elytra* as calculated from [22]. The test article was mounted at its center of gravity to an ATI Gamma load-cell. The load-cell was in turn mounted to the end of a STAUBLI TX2-90 robotic arm for automatic positioning of the test samples at the correct attitude

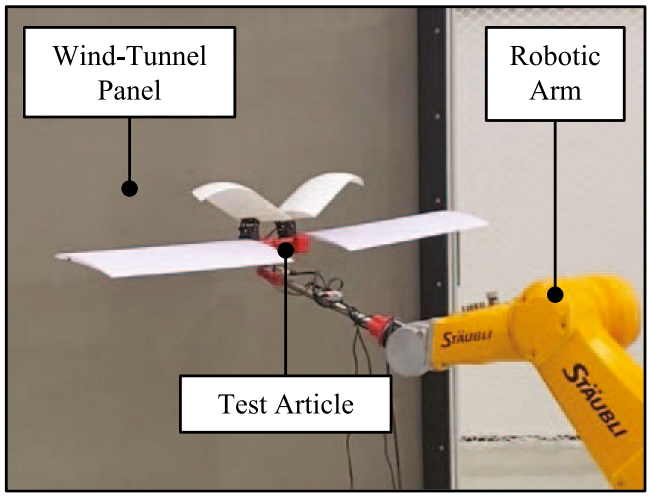

Fig. 4. Aerodynamics experimental setup. In the figure is depicted the test article with the hind-wings and the *elytra*, the robotic arm used to change the tested angle of attack and the front of the open wind-tunnel section.

(Fig. 4). For data logging, we used a National Instruments NI-DAQmx 9.5.1. Before each measurement sequence, the load-cell was zeroed at 0 m/s airspeed. Then, we set the tunnel to a mean wind speed of 8 m/s. We incremented the angle of attack from -4° to 20° in 2° steps. The angle of incidence was varied between -20° and 20° with a step of 10° and the dihedral was varied between 12° and 27° with a step of 5°. At each step, the loads were measured for 6 seconds at 1000 Hz. We used the combined area of the hind-wings and *elytra* (0.22 m^2) to calculate the aerodynamic coefficients. The wind tunnel raw data and the data analysis are provided as supplementary material.

The experiments indicated that there is not one single configuration that is optimal for all angles of attack of the hind-wings with *elytra* system (Fig. 5(A, B)). We observed that at a given angle of incidence, at high angles of attack, higher dihedral can perform better in terms of lift to drag ratio compared to lower dihedral, while this effect is reversed for lower angles of attack (Fig. 5 (B)). We also see that the highest efficiency configuration is achieved at 6° angle of attack, with 0° angle of incidence and 12° dihedral angle, while the lowest is achieved for 20° angle of attack, with 10° angle of incidence and 12° dihedral.

We selected the highest efficiency configuration for the hind-wings and *elytra* system to illustrate the performance of the hind-wings and *elytra* both individually and in synergy. For the beetles it has been shown that one of the *elytra* benefits is delaying stall by interacting with the hind-wings [24]. For this configuration of hind-wings and *elytra* at dihedral of 12° and 0°angle of incidence, and as presented in Fig. 7 we found that the *elytra* not only increase lift over the hind-wing on its own, but also delay the stall of the system from 14° without *elytra* to 20° with *elytra*.

The data collected as part of this experiment can be used to calculate a hypothetical cruise power required. We estimate the power required of a fixed wing UAV given by [25],

$$P_{CRUISE} = D_{CRUISE} * V_{CRUISE} \quad (1)$$

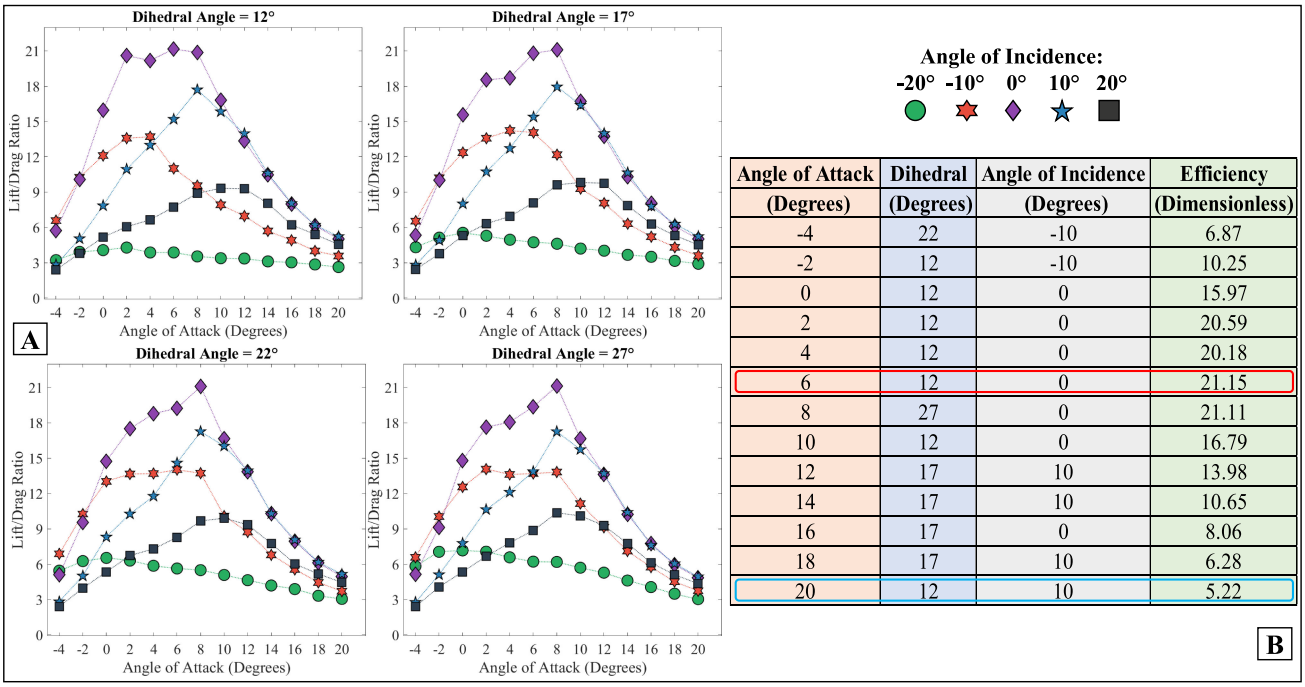

Angle of Attack (Degrees)	Dihedral (Degrees)	Angle of Incidence (Degrees)	Efficiency (Dimensionless)
-4	22	-10	6.87
-2	12	-10	10.25
0	12	0	15.97
2	12	0	20.59
4	12	0	20.18
6	12	0	21.15
8	27	0	21.11
10	12	0	16.79
12	17	10	13.98
14	17	10	10.65
16	17	0	8.06
18	17	10	6.28
20	12	10	5.22

B

Fig. 5. (A) The angle of incidence and dihedral were varied during the experiments as shown in Table I. In this graph we plot the angle of attack and the lift to drag ratio for each dihedral angle and each angle of incidence. (B) The integrated table presents the most efficient configuration for each angle of attack that was studied in the aerodynamic experiments. With the red rectangle we highlight the highest efficiency achieved and with the blue rectangle we highlight the lowest efficiency achieved.

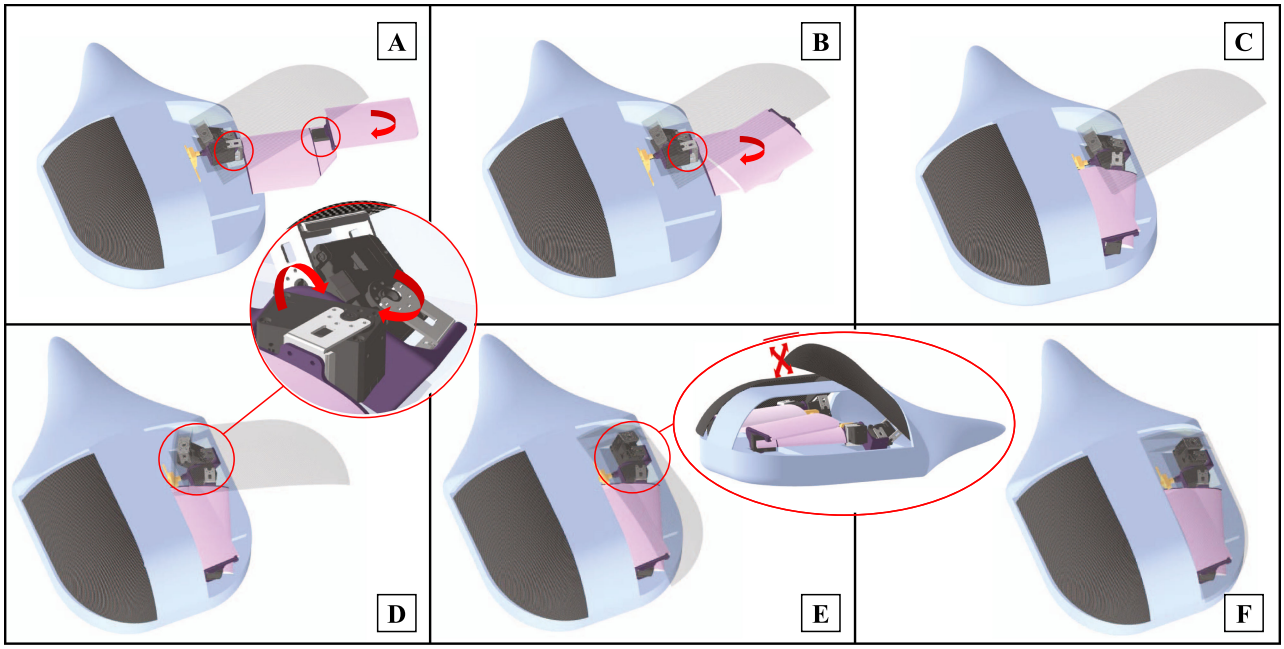

Fig. 6. Folding and unfolding of the hind-wings - *elytra* system. (A) The outer section of the hind-wing starts folding on top of the inner hind-wing section by enabling a one DoF actuator. (B) In less than 0.2 seconds, the one DoF actuator in the root of the hing-wing initiates folding of the whole wing section on top of the fuselage compartment. (C) Before the completion of the hind-wing folding, the 2 DoF actuators of the *elytron*, operate simultaneously. (D) The *elytron* starts approaching the fuselage. The actuators move with rotations presented in the zoom in detail. (E) The *elytron* folds on top of the hind-wing and thus fully enclose it within the compartment that the concave *elytron* surface and the fuselage create. The red arrows in the perspective view, indicate the direction of the *elytron* motion. (F) Similar to the beetles, the hind-wing now is completely enclosed and geometrically isolated from its surroundings and thus ready for ground locomotion [23]. The reverse procedure describes the unfolding of the wing system to their flight configuration.

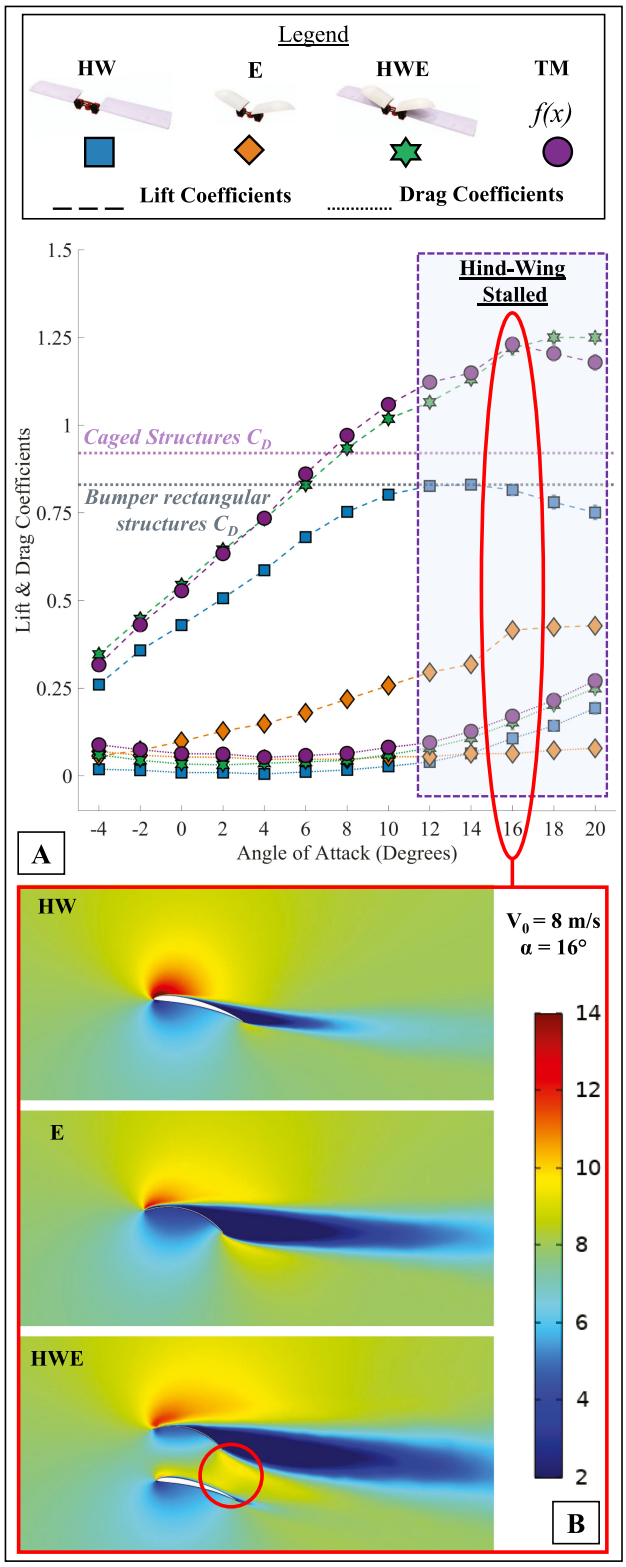

Fig. 7. (A) Experimental results and the theoretical model prediction as a graph of the aerodynamic coefficients and the angle of attack. Wind-tunnel experiments performed show the added lift that that *elytra* generate. The shaded area display the hind-wings post-stall domain. In the legend, HW for Hind-Wings, E for *Elytra*, HWE for Hind-Wings *Elytra* and TM for the Theoretical Model. The horizontal lines, represent the drag coefficients of existing protective solutions [26], [27]. (B) CFD experiments for the hind-wing, *elytron* and the hind-wing - *elytron* in the post stall angle of attack of 16°. The red circle indicates the region where the airflow over the hind-wing gets re-energized.

where D_{CRUISE} and V_{CRUISE} are the total drag and velocity in cruise flight respectively. Given a cruise angle of attack of 6 degrees, we found that with the elytra the power required is 2.65 W, while without it is 0.75 W (Fig. 7). This is an estimated 2.5 times increase in power requirement, however, state of the art caged structures would have a power required of 56.95 W (hind-wing drag plus caged structure drag in Fig. 7) which is around 20 times more than our solution.

The hind-wings and *elytra* system resembles a biplane configured aircraft, so we modeled the aerodynamics of test article with a standard biplane model. A good match between the biplane model and our experimental results would indicate that there is an existing aerodynamic model that could be applied to hind-wings and *elytra* systems rather than necessitate the development of a new one. We used the model presented by Jones *et al.* [28] where lift and drag coefficients are respectively modeled as,

$$C_{L_{total}} = \frac{A_{HW}C_{L_{HW}} + A_E C_{L_E}}{A_{HW} + A_E} \tag{2}$$

$$C_{D_{total}} = \frac{A_{HW}C_{D_{HW}} + A_E C_{D_E}}{A_{HW} + A_E} \tag{3}$$

where A_{HW} is the aerodynamic reference area of the hind-wings, A_E is the reference area of the *elytra*, $C_{L_{HW}}$ and $C_{D_{HW}}$ correspond to the lift and drag coefficients of the hind-wings and C_{L_E} and C_{D_E} correspond to the lift and drag coefficients of the *elytra*.

The experimental results show good agreement with the biplane model (Purple line in Fig. 7 (A). The root mean squared error of the theoretical model for the lift coefficients is 0.0013 and for the drag coefficients is 0.0005. In addition, Fig. 7 (A) also presents measured and estimated drag coefficients of existing protective solutions. To further investigate the aerodynamics between the hind-wing and the *elytra* system and possible interactions between the two wings in the post-stall region, we performed Computation Fluid Dynamic (CFD) experiments using COMSOL 5.5. We applied a Reynolds-averaged Navier-Stokes k-ϵ model in the 2D domain of the hind-wing, the *elytron*, and the hind-wing - *elytron* [29]. The geometrical model was meshed into approximately 12000 polygons. The inlet flow speed was set at 8 m/s. We varied the angle of attack between 12, 16 and 20 degrees. Fig. 7 shows the results for the experiment at 16 degrees. At all the measured angles, we observed that there is a reduction of the low velocity area of the hind-wing in the trailing edge region, an increase in the velocity region and a re-energization of the flow between the trailing edge of the hind-wing and the trailing edge of the *elytron* (red circle in Fig. 7). The proposed model from [28] assumes that interactions between the wings are negligible. Thus, we hypothesize that the observed interactions between the hind-wing and the *elytron* in the CFD results, justify the deviations from the proposed model that appear to be sovereign in the post stall region.

TABLE II
LINEAR REGRESSION FOR THE LIFT COEFFICIENTS

Coefficients	Estimate	pValue
Angle of Attack	0.031	**4.157e-103**
Dihedral	0.002	**0.012**
Angle of Incidence	-0.003	**2.717e-15**

TABLE III
LINEAR REGRESSION FOR THE DRAG COEFFICIENTS

Coefficients	Estimate	pValue
Angle of Attack	0.007	**4.486e-50**
Dihedral	3.456e-11	0.350
Angle of Incidence	-0.001	**2.149e-19**

To understand the relative importance of the experimental variables of angle of attack, angle of incidence and dihedral affects overall system performance, we study their individual effect in the lift and drag coefficients using a linear regression model. With this analysis we can highlight the parameter that has the largest impact on the flight efficiency, which in turn will inform future designers of such systems on the importance of each parameter. We performed two linear regression fits on the experimental results to study the linear effects of the variables. One regression was performed between the three angles and the lift coefficient and the other regression was performed between the same angles and the drag coefficient. Assuming that statistical significance exist with pValue less than 0.05, the first regression results (Table II), displayed a statistically significant effect of all of the angles on the lift coefficient. The most significant factor is the angle of attack followed by the angle of incidence and finally the dihedral. The second linear regression results (Table III), display a significant effect of both angle of attack and angle of incidence, but not the dihedral. The order of importance for drag coefficient is first the angle of attack then the angle of incidence.

III. DESIGN, FABRICATION AND EXPERIMENTATION WITH HERCULIS

In order to illustrate the value of the proposed protective concept, we fabricated the drone demonstrator, HercuLIS. The drone has the ability to fold its wings rapidly (less than half a second) and thus during the approach to a dangerous environment, encapsulate the folding wings beneath the *elytra* to protect them. When locomoting on the ground the hind-wings are folded and protected by the *elytra*. When the vehicle is clear from obstacles and on appropriate ground for take-off, it unfolds the wings and is ready to fly. The hind-wings were sized to fit underneath the *elytra* and have a folding ratio (planform area of the wing closed to wing open) of about 39%. The wing length of the hind-wing was reduced to 0.35 m to allow the full encapsulation with the current folding method. The length of the *elytron* was increased from 0.28 m to 0.33 m so that the surface area of the *elytra* that was in the airflow is the same as the amount of surface area of the *elytra* that was in the wind-tunnel. The concave compartment that the elliptical shape of the *elytra* and the fuselage forms is used to completely encapsulate the folding hind-wings (Fig. 6). The geometry of the *elytra* was

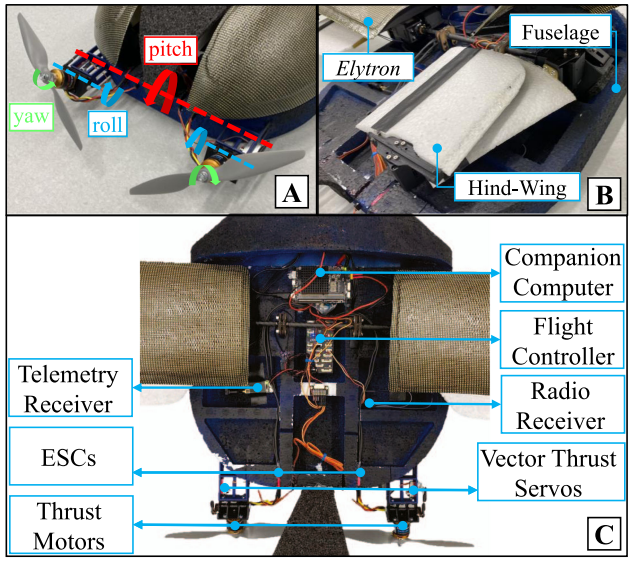

Fig. 8. (A) The vectored thrust motors controlling pitch when moving symmetrically, roll when moving asymmetrically and yaw with differential thrust. (B) Detail of folded hind-wing on top of the fuselage with the *elytra* on extended position. (C) HercuLIS consists of a blended body fuselage manufactured from Expanded Polypropylene (EPP) foam, dual vectored thrust motor propulsion system, an autopilot with data logging, and a companion computer for controlling the hind-wings and *elytra* servos.

derived as a geometric abstraction of the beetle's *elytra*. We scaled by a factor of ten the chord and length dimension of the animal's *elytra* to the size range of a MAV [12], [19]. The shape of the curve was derived as a section of an ellipsoid defined by a linear and a circular part. The 3D model of the *elytron* is shared as supplementary material. The *elytra* are mounted on two, 2 DoF servomotors that reorient their position to cover the folded hind-wings on the back of the fuselage. HercuLIS electronic components are labeled in Fig. 8. The communication between the components is achieved through a ROS-node in the ROS network that receives the user inputs and commands the *elytra* and the hind-wings servos to fold or unfold.

For the fabrication of the main wings of the demonstrator we used EPP foam due to the ease of manufacturability and robustness. The two 2 DoF actuators were mounted in such an orientation that upon actuation the *elytra* were completely encapsulating the hind-wings (Red arrows in Fig. 6). The desired angle of incidence was achieved with a fixed 3D printed interface fabricated with the material and methods used for the test article, while the folding of the *elytra* and the regulation of the dihedral angle, was achieved with two XC-430-W250-T servos. For reducing the structural weight of the demonstrator, we fabricated the *elytra* from hybrid carbon Kevlar fabric with a 3 mm honeycomb core for added stiffness. For the fuselage of the demonstrator, we used EPP foam that was machined with a Modela Pro II MDX-540S 3D milling machine in six parts that were attached together with UHU POR glue. For the propulsion system, two commercially available electric motors, AXI 2217/12 GOLD LINE V2 were used with 9x4.5 APC propellers and 60 A electronic speed controller from Hobbywing. The vector thrust components were fabricated from plywood

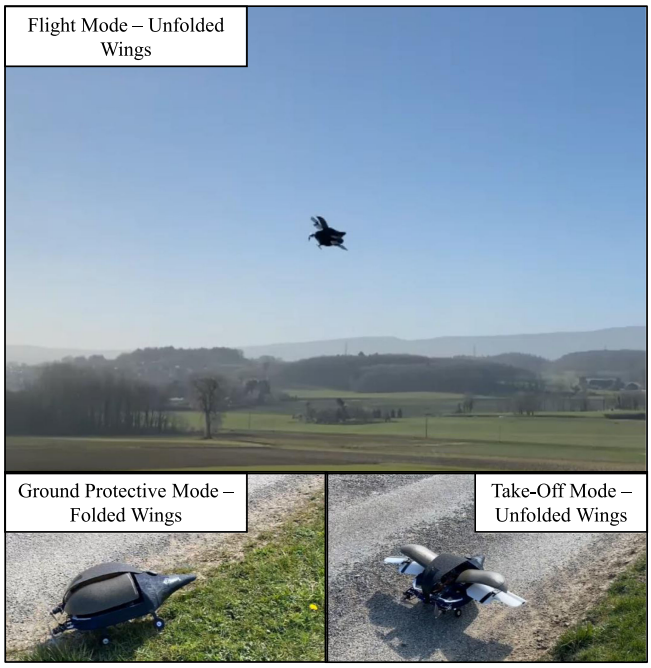

Fig. 9. HercuLIS in field tests.

and 3D printed ABS components. The motors thrust vector was adjusted in pitch by two X08H V5.0 digital high voltage servos from KST. The pusher configuration was chosen in order to avoid flow interaction of the wings and the propeller. We used a Futaba R2000SBM receiver and a Futaba 12 K transmitter for the manual control of the drone. For powering the system we used a 3-cell Hacker lithium polymer battery pack with a 3800 mAh capacity. An overview of the electrical setup can be found in Fig. 8 (C). In the HercuLIS vehicle, the folding and unfolding were manually controlled. The pilot deployed or retracted the wings depending on the mode of locomotion. In future iterations of the vehicle the folding, unfolding and the in-flight wing configuration, will be controlled by the autopilot.

The goal of the demonstrator was to show that despite the mechanical complexity, a folding hind-wing *elytra* system can be integrated into a working multimodal platform while displaying basic operational capabilities. The platform would need further optimization such as weight and volume reduction and aerodynamic optimization such that the blended fuselage design does not interfere with the aerodynamics of the hind-wing *elytra*.

Field experiments of HercuLIS were conducted with the goal of demonstrating the dual-wing protective system in ground locomotion with the hind-wings folded below the *elytra* for protection and hind-wings and *elytra* deployed for flight (Fig. 9). The two flight test flights were conducted in calm wind conditions of approximately 1.5 m/s. The vehicle was hand launched as there was no adequate runway to take-off. The experiments showed that the vehicle is capable of flying and of locomoting on the ground by means of four foam wheels. The propellers produce the necessary thrust for forward motion, while the differential thrust from the propellers allow the vehicle to steer. Although in the current implementation that vehicle's clearance to the ground is 10 cm, it could successfully locomote over uneven terrain with 5–7 cm high grass.

IV. Conclusions

In this letter, we described a novel insect inspired approach for protecting winged drones in challenging environments. Similar to beetles, we used a secondary set of wings akin to *elytra*, that when swept back, encapsulate a set of hind-wings that are folded into the fuselage. We validated the feasibility of the proposed solution in a flying platform named HercuLIS. During the field experiments we validated the capabilities of the platform for folding its hind-wings and *elytra* during on uneven and unstructured ground, and thus protecting the hind-wings surfaces and actuators from external damage namely spicular surfaces or ground collisions. The experiments provided insights on the *elytra* lift and drag generation and in the future, the geometry of the system can be optimised to achieve better performance.

The solution proposed here could fit as a design choice for vehicles with different mission profiles. The current work and our previous work on the hind-wings and *elytra* systems validated the benefits of such systems compared to existing solutions [30]. In both studies we found that the biplane model provides an adequate approximation for the aerodynamic forces in the regions of Re 68000 and Re 90000 [30]. Multi-modal locomotion drones could benefit when using *elytra* to protect their main wings when locomoting on a challenging terrain. Morphing wing drones could benefit by using *elytra* wings to protect their fragile wing surfaces and morphing mechanisms. Further work can explore integrating different *elytra* shapes to maximize performance, or hind-wings with higher folding ratios. Moreover, a third degree of freedom in the *elytra* actuation, could increase the possible geometric adaptations of the *elytra* during flight and might be a sustainable way of achieving greater performance in a wider flight regime. In nature, beetles use their *elytra* to achieve multiple goals beyond collision resilience. For example, camouflage [31], thermoregulation [13], humidity control [13], control through passive flight stability [32], and radiation control [33] according to the physical or chemical properties of the *elytra*. We also believe that with structural and chemical adaptation, it is possible to integrate further capabilities in the *elytra* to enable future robots to perform multiple other functionalities that are similar to what the *Coleoptera* have utilised to survive for millions of years in challenging and hazardous environments.

Acknowledgment

The authors are grateful for the engineering help provided by Simon Honigmann, Nathan Müller, Olexandr Gudozhnik and Angelika Romanou.

References

[1] A. Briod, P. Kornatowski, J.-C. Zufferey, and D. Floreano, "A collision-resilient flying robot," *J. Field Robot.*, vol. 31, no. 4, pp. 496–509, 2014, [Online]. Available: https://onlinelibrary.wiley.com/doi/pdf/10.1002/rob.21495. [Online]. Available: https://onlinelibrary.wiley.com/doi/abs/10.1002/rob.21495

[2] C. J. Salaan, K. Tadakuma, Y. Okada, Y. Sakai, K. Ohno, and S. Tadokoro, "Development and experimental validation of aerial vehicle with passive rotating shell on each rotor," *IEEE Robot. Automat. Lett.*, vol. 4, no. 3, pp. 2568–2575, Jul. 2019.

[3] D. Kumar, S. F. Ali, and A. Arockiarajan, "Structural and aerodynamics studies on various wing configurations for morphing," *IFAC-PapersOnLine*, vol. 51, no. 1, pp. 498–503, 2018. [Online]. Available: https://linkinghub.elsevier.com/retrieve/pii/S2405896318302489

[4] A. Klaptocz, A. Briod, L. Daler, J.-C. Zufferey, and D. Floreano, "Euler spring collision protection for flying robots," in *Proc. IEEE/RSJ Int. Conf. Intell. Robots Syst.*, 2013, pp. 1886–1892. [Online]. Available: http://ieeexplore.ieee.org/document/6696606/

[5] A. Kalantari and M. Spenko, "Design and experimental validation of HyTAQ, a hybrid terrestrial and aerial quadrotor," in *Proc. IEEE Int. Conf. Robot. Automat.*, 2013, pp. 4445-4450, iSSN: 1050–4729.

[6] P. Sareh, P. Chermprayong, M. Emmanuelli, H. Nadeem, and M. Kovac, "Rotorigami: A rotary origami protective system for robotic rotorcraft," *Sci. Robot.*, vol. 3, no. 22, Sep. 2018, Art. no. eaah 5228. [Online]. Available: https://robotics.sciencemag.org/lookup/doi/10.1126/scirobotics.aah5228

[7] D. Gandhi, L. Pinto, and A. Gupta, "Learning to fly by crashing," in *Proc. IEEE/RSJ Int. Conf. Intell. Robots Syst.*, 2017, pp. 3948-3955, iSSN: 2153–0866.

[8] "eBee X," Sept. 2018. [Online]. Available: https://www.sensefly.com/drone/ebee-x-fixed-wing-drone/

[9] A. K. Stowers and D. Lentink, "Folding in and out: Passive morphing in flapping wings," *Bioinspiration Biomimetics*, vol. 10, no. 2, Mar. 2015, Art. no. 0 25001. [Online]. Available: http://stacks.iop.org/1748-3190/10/i=2/a=025001?key=crossref.a8a11ecfbeb3c732dbd277e7e5d44c11

[10] Y. Chen, S. Xu, Z. Ren, and P. Chirarattananon, "Collision resilient insect-scale soft-actuated aerial robots with high agility," *IEEE Trans. Robot.*, vol. 37, no. 5, pp. 1752–1764, Oct. 2021.

[11] L. Daler, S. Mintchev, C. Stefanini, and D. Floreano, "A bioinspired multi-modal flying and walking robot," *Bioinspiration Biomimetics*, vol. 10, no. 1, Jan. 2015, Art. no. 016005. [Online]. Available: http://stacks.iop.org/1748-3190/10/i=1/a=016005?key=crossref.f305bd49cb1d6cb9a009c91104061e28

[12] L. C. Johansson, S. Engel, E. Baird, M. Dacke, F. T. Muijres, and A. Hedenström, "Elytra boost lift, but reduce aerodynamic efficiency in flying beetles," *J. Roy. Soc. Interface*, vol. 9, no. 75, pp. 2745–2748, Oct. 2012. [Online]. Available: https://royalsocietypublishing.org/doi/10.1098/rsif.2012.0053

[13] D. M. Linz, A. W. Hu, M. I. Sitvarin, and Y. Tomoyasu, "Functional value of elytra under various stresses in the red flour beetle, Tribolium castaneum," *Sci. Rep.*, vol. 6, no. 1, pp. 1–10, Oct. 2016, number: 1 Publisher: Nature Publishing Group. [Online]. Available: https://www.nature.com/articles/srep34813

[14] T. Q. Le *et al.*, "How could beetle's elytra support their own weight during forward flight?" *J. Bionic Eng.*, vol. 11, no. 4, pp. 529–540, Dec. 2014. [Online]. Available: http://link.springer.com/10.1016/S1672-6529(14)60065-2

[15] B. Lee, H. Park, and S.-T. Kim, "Three-dimensional wing behaviors of a rhinoceros beetle during takeoff flights," *J. Mech. Sci. Technol.*, vol. 29, no. 12, pp. 5281–5288, Dec. 2015. [Online]. Available: http://link.springer.com/10.1007/s12206-015-1130-x

[16] W. Marcińczyk, "Beetle," [Online]. Available: https://unsplash.com/photos/RXV1X3wEe8k

[17] L. Frantsevich, "Geometry of elytra opening and closing in some beetles (coleoptera, polyphaga)," *J. Exp. Biol.*, vol. 208, no. 16, pp. 3145–3158, Aug. 2005. [Online]. Available: http://jeb.biologists.org/cgi/doi/10.1242/jeb.01753

[18] SgH, "Stag Beetle," [Online]. Available: https://pixabay.com/photos/stag-beetle-tree-wing-644129/

[19] M. Hassanalian and A. Abdelkefi, "Classifications, applications, and design challenges of drones: A review," *Prog. Aerosp. Sci.*, vol. 91, pp. 99–131, May 2017. [Online]. Available: http://www.sciencedirect.com/science/article/pii/S0376042116301348

[20] "WindShape - drone test equipment and services - wind tunnel," [Online]. Available: https://www.windshape.ch/

[21] E. Ajanic, M. Feroskhan, S. Mintchev, F. Noca, and D. Floreano, "Bioinspired wing and tail morphing extends drone flight capabilities," *Sci. Robot.*, vol. 5, no. 47, Oct. 2020, Art. no. eabc 2897. [Online]. Available: https://robotics.sciencemag.org/lookup/doi/10.1126/scirobotics.abc2897

[22] J. Anderson, *Fundamentals of Aerodynamics*. New York, NY, USA: McGraw-Hill, 2010. [Online]. Available: https://books.google.de/books?id=xwY8PgAACAAJ

[23] J. Goczał, R. Rossa, and A. Tofilski, "Elytra reduction may affect the evolution of beetle hind wings," *Zoomorphology*, vol. 137, no. 1, pp. 131–138, Mar. 2018. [Online]. Available: http://link.springer.com/10.1007/s00435-017-0388-1

[24] T. Q. Le *et al.*, "Improvement of the aerodynamic performance by wing flexibility and elytra-hind wing interaction of a beetle during forward flight," *J. Roy. Soc. Interface*, vol. 10, no. 85, Aug. 2013, Art. no. 20130312. [Online]. Available: https://royalsocietypublishing.org/doi/10.1098/rsif.2013.0312

[25] W. F. Phillips, *Mechanics of Flight*. Hoboken, NJ, USA: John Wiley & Sons, Inc., 2004.

[26] P. Kornatowski, S. Mintchev, and D. Floreano, "An origami-inspired cargo drone," in *Proc. IEEE/RSJ Int. Conf. Intell. Robots Syst.*, . 2017, pp. 6855–6862, iSSN: 2153-0866. [Online]. Available: https://ieeexplore.ieee.org/document/8206607

[27] C. J. Salaan, Y. Okada, K. Hozumi, K. Ohno, and S. Tadokoro, "Improvement of UAV's flight performance by reducing the drag force of spherical shell," in *Proc. IEEE/RSJ Int. Conf. Intell. Robots Syst.*, 2016, pp. 1708-1714, iSSN: 2153–0866. [Online]. Available: https://ieeexplore.ieee.org/document/7759274

[28] R. Jones, D. J. Cleaver, and I. Gursul, "Aerodynamics of biplane and tandem wings at low reynolds numbers," *Exp. Fluids*, vol. 56, no. 6, p. 124, Jun. 2015. [Online]. Available: https://doi.org/10.1007/s00348-015-1998-3

[29] H. K. Versteeg and W. Malalasekera, *An Introduction to Computational Fluid Dynamics: The Finite Volume Method*. Essex, UK: Pearson Education, 2007. [Online]. Available: https://books.google.de/books?id=RvBZ-UMpGzIC&lpg=PR11&ots=u3yWA9BkIe&dq=An%20Introduction%20to%20Computational%20Fluid%20Dynamics%3A%20The%20Finite%20Volume%20Method.%20Pearson%20Education&lr&hl=el&pg=PA87#v=onepage&q=An%20Introduction%20to%20Computational%20Fluid%20Dynamics:%20The%20Finite%20Volume%20Method.%20Pearson%20Education&f=false

[30] C. Vourtsis, V. Casas Rochel, F. Ramirez Serrano, W. Stewart, and D. Floreano, "Insect inspired self-righting for fixed-wing drones," *IEEE Robot. Automat. Lett.*, vol. 6, no. 4, pp. 6805–6812, Jul. 2021

[31] B. D. Wilts, K. Michielsen, J. Kuipers, H. De Raedt, and D. G. Stavenga, "Brilliant camouflage: photonic crystals in the diamond weevil, Entimus imperialis," *Proc. Roy. Soc. B: Biol. Sci.*, vol. 279, no. 1738, pp. 2524–2530, Jul. 2012, publisher: Royal Society. [Online]. Available: https://royalsocietypublishing.org/doi/10.1098/rspb.2011.2651

[32] M. M. D. Souza and D. E. Alexander, "Passive aerodynamic stabilization by beetle elytra (*wing covers*)," *Physiol. Entomol.*, vol. 22, no. 2, pp. 109–115, 1997, [Online]. Available: https://onlinelibrary.wiley.com/doi/pdf/10.1111/j.1365-3032.1997.tb01147.x. [Online]. Available: https://onlinelibrary.wiley.com/doi/abs/10.1111/j.1365-3032.1997.tb01147.x

[33] E. Cuesta and J. M. Lobo, "Visible and near-infrared radiation may be transmitted or absorbed differently by beetle elytra according to habitat preference," *PeerJ*, vol. 7, Nov. 2019, Art. no. e 8104, publisher: PeerJ Inc. [Online]. Available: https://peerj.com/articles/8104